Neural Networks for Estimating Storm Surge Loads on Storage Tanks

Carl Bernier
Graduate Student, Dept. of Civil and Environmental Engineering, Rice University, Houston, USA

Jamie E. Padgett
Associate Professor, Dept. of Civil and Environmental Engineering, Rice University, Houston, USA

ABSTRACT: Failures of aboveground storage tanks (ASTs) during past storm surge events have highlighted the need to evaluate the reliability of these structures. To assess the reliability of ASTs, an adequate estimation of the loads acting on them is first required. Although finite element (FE) models are typically used to estimate storm surge loads on ASTs, the computational cost of such numerical models can prohibit their use for reliability analysis. This paper explores the use of computationally efficient surrogate models to estimate storm surge loads acting on ASTs. First, a FE model is presented to compute hydrodynamic pressure distributions on ASTs subjected to storm surge and wave loads. A statistical sampling method is then employed to generate samples of ASTs with different geometries and load conditions, and FE analyses are performed to obtain training, validation, and testing data. Using the data, an Artificial Neural Network (ANN) is developed and results indicate that the trained ANN yields accurate estimates of hydrodynamic pressure distributions around ASTs. More importantly, the ANN model requires less than 0.5 second to estimate the hydrodynamic pressure distribution compared to more than 30 CPU hours needed for the FE model, thereby greatly facilitating future sensitivity, fragility, and reliability studies across a broad range of AST and hazard conditions. To further highlight its predictive capability, the ANN is also compared to other surrogate models. Finally, a method to propagate the error associated with the ANN in fragility or reliability analyses of ASTs is presented.

1. INTRODUCTION

Aboveground storage tanks (ASTs) have suffered damage resulting in the release of hazardous chemicals during almost every major storm in the United States (US) (Sengul et al. 2012). During Hurricanes Katrina and Rita, 26 million liters of oil were spilled due to AST failures (Godoy 2007). More recently, during Hurricane Harvey, the failure of two ASTs caused the release of one million liters of gasoline in the Houston area (Bernier and Padgett 2018b). ASTs are generally constructed from thin steel plates forming a vertical cylinder. While this geometry makes them economical and able to efficiently withstand internal pressure, it also leaves them vulnerable to external loads such as wind and storm surge. In fact, three failure modes are generally observed during storms: (i) wind-induced buckling; (ii) surge-induced buckling; and (iii) dislocation from the ground due to storm surge (Godoy 2007).

In order to assess the structural safety or reliability of ASTs, and thereby evaluate the risks posed by ASTs during storm events, an adequate estimation of the loads acting on ASTs is crucial. Wind, hydrostatic, and hydrodynamic pressure distributions are required to determine the buckling strength and assess stability against dislocation. While simple models are readily available for hydrostatic and wind pressures on ASTs (Godoy 2016), less information is available regarding the hydrodynamic pressures associated with wave loads and current. Existing analytical models for hydrodynamic loads, such as the Morison equation (Morison et al. 1950), are generally restricted to small-scale cylinders and linear waves. For large-scale cylinders and nonlinear waves, such as ASTs and waves

observed during a storm, computational fluid dynamics (CFD) analyses are usually employed for accurate solutions (Wang and Wu 2010). However, such numerical analyses are generally computationally expensive, and their use is prohibitive for reliability analysis, which typically requires a large number of simulations.

This paper aims to develop a computationally efficient surrogate model to estimate hydrodynamic pressures acting on ASTs during storm surge. For this purpose, this study relies on Artificial Neural Networks (ANNs) given their powerful predictive capability for highly non-linear data (Chojaczyk et al. 2015). Also, while several studies have employed ANNs to accurately and efficiently perform reliability analysis (Chojaczyk et al. 2015; Hurtado and Alvarez 2001), estimate wind loads (Chen et al. 2002), or forecast storm and wave conditions (Lee 2006; Tsai and Tsai 2009), very few studies have employed ANNs to evaluate hydrodynamic loads on structures. Some studies have used ANNs to predict wave forces on simple structures, such as breakwater (Mase and Kitano 1999), but no study has used ANNs to estimate hydrodynamic pressure distributions on more complex structures; predicting pressure distributions is essential to assess buckling strength. This study is one of the first to highlight the capability of ANNs to accurately estimate hydrodynamic pressure distributions, rather than simply wave forces, on large-scale structures.

Section 2 of this paper presents the numerical model employed to estimate hydrodynamic pressures on ASTs subjected to storm surge and wave loads. Section 3 then presents the statistical sampling approach used to train the ANN surrogate model. Section 4 presents the derived ANN, its performance on test data, and a comparison with other surrogate modeling techniques. Finally, Section 5 presents models to propagate the error associated with the ANN within a fragility or reliability analysis.

2. FINITE ELEMENT MODEL

The CFD model employed to estimate hydrodynamic pressures on ASTs and develop the surrogate model is adopted from Bernier and Padgett (2018a) and is presented in Figure 1. The model was developed in *LS-Dyna* (LSTC 2016), a commercial finite-element (FE) software, using the Arbitrary-Lagrangian Eulerian (ALE) method. Both the water and air fluid elements are governed by the Navier-Stokes equations, while the water-air interface is tracked using an ALE formulation. Taking advantage of symmetry, only half of the domain is modeled. Waves and current are generated by prescribing the velocity at the inflow boundary and are absorbed at the outflow boundary. Slip boundary conditions are employed for all other boundaries as well as at the tank shell location to simulate a rigid AST behavior. As shown in Figure 1, the extent of the domain is a function of the diameter (D) of the AST under analysis. Additional details on the FE model and its validation against experimental results can be found in Bernier and Padgett (2018a).

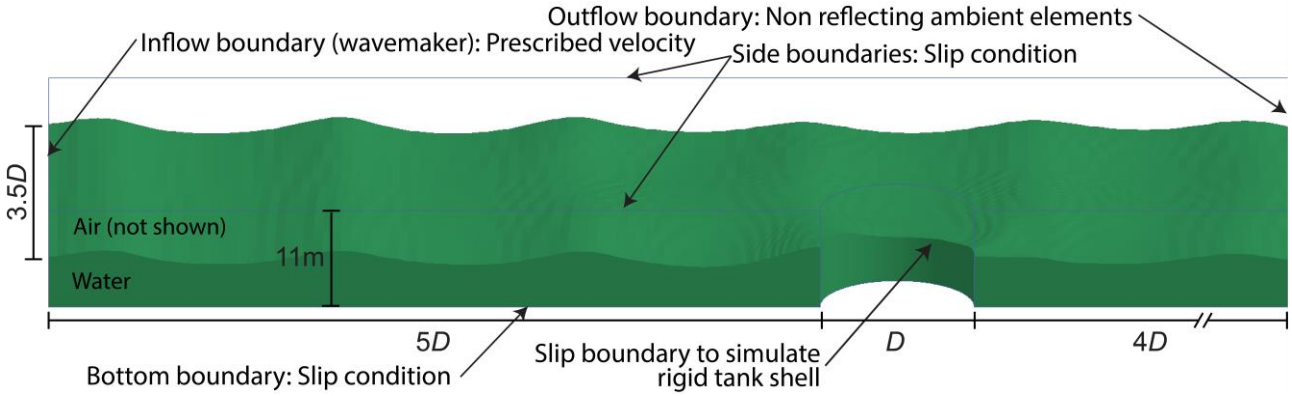

Figure 1. Overview of the CFD model to estimate hydrodynamic pressure on ASTs.

The waves and current velocity profiles at the inflow boundary are obtained from Fenton's wave theory (Fenton 1988); this theory is accurate for the ranges of wave conditions discussed in the next section. FE analyses are performed for a duration of 200 seconds to generate a sufficient number of waves to obtain a steady state solution. Depending on the diameter of the AST, which can range between 5 and 60 m as detailed in the next section, the computational cost of this FE model varies between 30 and 90 CPU hours.

3. EXPERIMENTAL DESIGN

The computational cost of the above FE model highlights the need to develop a more efficient surrogate model to enable reliability analyses of ASTs during storm events. Developing a surrogate model first requires the generation of training points to efficiently span the space of parameters. In this study, Latin Hypercube Sampling (LHS) (Mckay et al. 1979) is employed to generate a space-filling experimental design. The parameters considered in the design and their ranges are presented in Table 1. All parameters are assumed to be uniformly distributed as recommended when training a surrogate model (Hurtado and Alvarez 2001).

Table 1: Parameters in the LHS design.

Parameter	*Range*	*Unit*
Diameter (D)	*5 – 60*	*m*
Surge height (S)	*1.0 – 7.5*	*m*
Wave height (H_w)	*0.0 – 2.0*	*m*
Wave period (T_w)	*3.5 – 6.0*	*s*
Current velocity (U)	*0.0 – 1.5*	*m/s*

The ranges of surge and wave parameters presented in Table 1 are obtained from the simulations of historic and synthetic storms in and around the Houston Ship Channel (HSC) in Texas, the largest petrochemical complex in the US with more than 4,600 ASTs. The simulations were performed using *ADCIRC+ SWAN* (Luettich and Westerink 2004), by The Computational Hydraulics Group at the University of Texas at Austin (Dawson 2017), for Hurricane Ike and for two synthetic storms which produce approximately 100- and 500-year storm surge events in the HSC. The range of AST diameters is obtained from Bernier et al. (2017).

A total of 240 samples are generated using LHS; 200 samples are used to train the surrogate model, 20 to validate the training, and 20 to test its performance. When generating the samples, the ratios H_w/S and H_w/λ_w, where λ_w is the wavelength, are limited to 0.65 and 0.14 respectively to ensure the generation of realistic waves (Fenton 1988). For each sample, a finite element analysis is performed, and the hydrodynamic (i.e., total pressure minus the hydrostatic pressure) pressure distribution when a wave impacts the tank and the horizontal force is maximum is extracted around the AST circumference (θ) and along the AST height (h). Figure 2 shows an example of hydrodynamic pressure distribution for D = 28.4 m, S = 5.8 m; H_w = 1.8 m, T_w = 4.6 s, and U = 0.65 m/s.

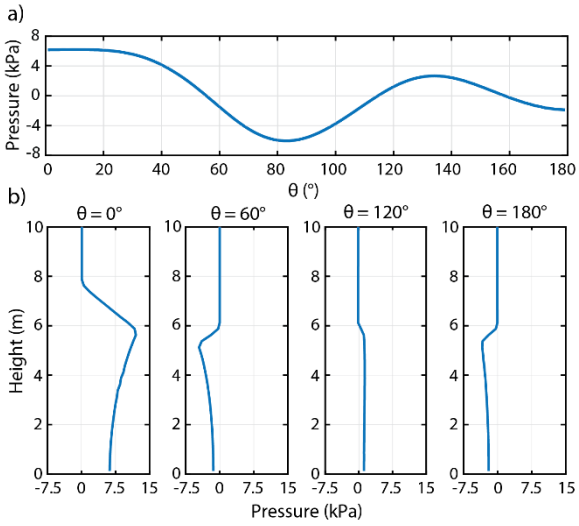

Figure 2: Hydrodynamic pressure distribution for a training sample. Pressure distribution: a) around the circumference at the base; b) along the height.

For each sample, the hydrodynamic pressure is extracted on a grid of 102 points along the AST circumference and 40 points along the AST height for a total of 4,080 pressure points per sample. 816,000 data points in total are used to train the surrogate model, while 81,600 data points are used to validate or test it.

4. SURROGATE MODELING

The surrogate model is developed with the results from the LHS samples. As shown in Eq. (1), the surrogate model should estimate the hydrodynamic pressure (P_d) at a point (θ, h) on an AST with diameter D and as a function of the surge and wave parameters (i.e. S, H_w, T_w, and U).

$$\text{Input: } \{D, S, H_w, T_w, U, \theta, h\} \mapsto \text{Output: } \{P_d\} \quad (1)$$

ANN is the surrogate modeling technique employed here, as ANNs are capable of accurately approximating nonlinear functions similar to the one shown in Fig. 2 (Chen et al. 2002; Tsai and Tsai 2009).

4.1. Overview of Neural Network

ANNs are nonlinear computing systems composed of interconnected processing units, usually called neurons. As shown in Fig. 3, neurons are organized into layers, and each neuron has weighted connections to the other neurons in adjacent layers to create the network.

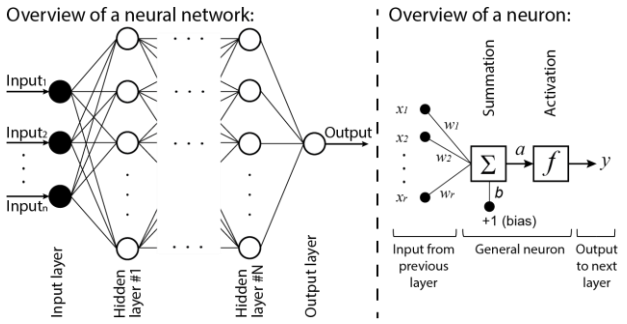

Figure 3: Overview of an Artificial Neural Network.

In the input layer, no operations are performed. The input data is simply fed to the first hidden layer. Herein, there are seven input neurons corresponding to the seven input parameters in Eq. (1). The processing of the data occurs in the hidden layers. In a hidden layer neuron, the data (x) from the previous layer neurons are affected by weights (w) and summed to obtain the activation value (a) of the neuron as shown in Eq. (2) and Figure 3.

$$a = \sum_{i=1}^{r} w_i x_i + b \quad (2)$$

In this equation, r is the number of neurons in the previous layer and b is a bias term. The output y of the neuron is then obtained as $y = f(a)$, where $f(\cdot)$ is an activation function. While numerous activation functions are available, the one adopted here is the log-sigmoid function. The outputs of all of the neurons of a hidden layer are then fed to the next hidden layer, and so on. The number of hidden layers and number of neurons per layer defines the performance of the ANN as detailed below. Lastly, the output layer transforms the data from the last hidden layer into the desired quantity, which here is P_d. The output neuron is similar to a hidden layer neuron and any activation function can be used; a linear activation function is employed here given its common use for regression problems (Hurtado and Alvarez 2001).

4.2. Network training and architecture

The training of an ANN consists of first initializing the network weights and biases and feedforwarding the training data to generate the output. In this study, the weights and biases are randomly initialized. The output error (i.e., the mean squared error (MSE)) is then computed and backpropagated in the network to adjust the weights and biases using a backpropagation algorithm. With the updated weights and biases, the procedure is then repeated to minimize the error of the surrogate model on P_d. The Levenberg-Marquardt backpropagation algorithm, available in MATLAB (MathWorks 2016), is adopted here because of its high efficiency for large datasets.

While the training dataset is used to determine the network weight and bias values, the validation dataset is used to determine when to stop the training and ensure that the ANN does not overfit the data; the validation dataset is not used to estimate the weights and biases. The test dataset is not used during the training phase and is only used to evaluate the performance of the ANN once it is trained. The errors on both the training and validation datasets are monitored at each iteration. Both errors are typically expected to decrease; however, if the validation error increases for more than six consecutive iterations, while the training

error continues to decrease, the training is stopped to avoid overfitting. The final weights and biases correspond to the values when the validation error is minimum.

The architecture of the ANN is defined by performing a parameter sweep. ANNs with 1, 2, 3, and 4 hidden layers as well as 10, 20, 30, and 40 neurons per layer are trained. Given the random nature of the initial weights, training the same ANN multiple times will not yield the same performance. For each possible architecture, 10 ANNs are trained and only the one with the best performance on the test data is used for comparison with the other architectures. The training time of the ANNs varies between 0.5 and 12 CPU hours. Based on the parameter sweep results, the network with the best performance has three hidden layers with 30 neurons per layer; this ANN is retained as the surrogate model to estimate hydrodynamic pressures on ASTs.

4.3. Performance of the Neural Network

The performance of the ANN on the test data is illustrated in Figures 4 and 5. Figure 4 shows the correlation between the ANN outputs and the *LS-Dyna* results. A very good fit is observed as the ANN can predict pressures with a R^2 value of 0.999. Figure 5 provides an example of the ANN performance on one of the test samples; the properties of the test sample are: D = 36.4 m, S = 1.5 m; H_w = 0.3 m, T_w = 5.3 s, and U = 0.1 m/s. The mean error for nonzero pressure points is 8.6% for this sample. Error statistics for the whole test dataset are presented in Table 2. Overall, results in this table highlight the adequate accuracy and predictive capability of the ANN to estimate hydrodynamic pressures around ASTs.

Table 2: Error statistics for the entire test dataset and for nonzero pressure points

Statistic	*Error*
Mean value	*5.4%*
Median value	*2.2%*
25th percentile value	*0.8%*
75th percentile value	*5.9%*
90th percentile value	*14.5%*
95th percentile value	*19.8%*

Another important metric to assess the performance of the ANN is the computational time required to estimate the hydrodynamic pressure distribution around an AST. With the ANN, approximately 0.3 seconds are required to estimate the entire pressure distribution (i.e. 4,080 pressure points) around an AST, which is significantly shorter than the minimum 30 CPU hours required for the FE model presented in Section 2 and highlights the efficiency of the surrogate model.

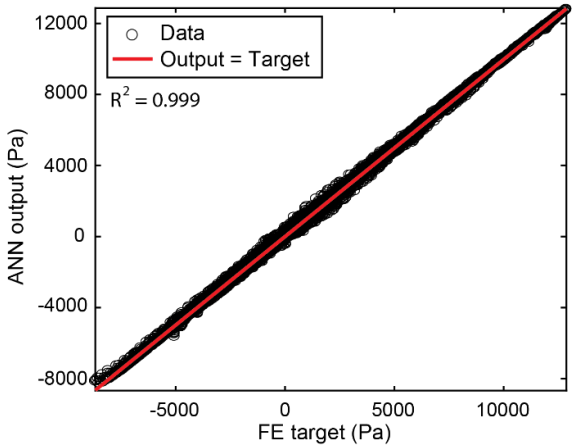

Figure 4: Comparison between target (LS-Dyna) and output (ANN) pressure for the test data.

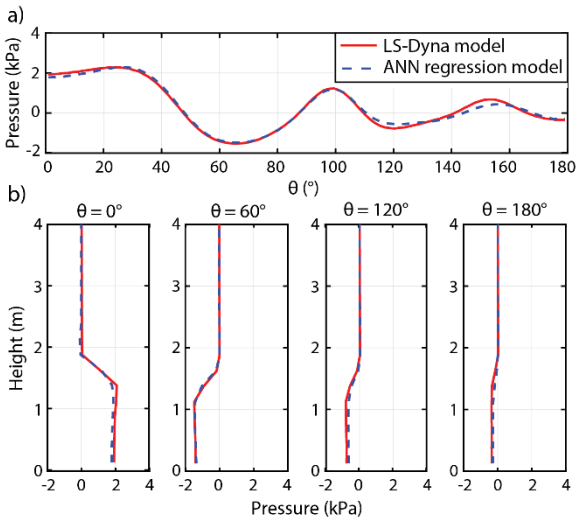

Figure 5: Performance of the ANN on a test sample.

4.4. Comparison with other surrogate models

To further demonstrate its performance, the ANN model is compared with three other surrogate modeling techniques commonly used to

approximate nonlinear data or FE models. The three techniques are: (i) Multivariate Adaptive Regression Splines (MARS) for which the output is predicted by a weighted sum of piecewise adaptive basis functions; (ii) Radial Basis Functions Network (RBFN) which is similar to the above ANN, but has a radial basis function as the activation function; and (iii) Kriging regression, for which the outputs are modeled by a Gaussian process with a correlation function.

Additional details on these surrogate modeling methods can be found in Jin et al. (2001), Lataniotis et al. (2018), among other relevant references. As for the ANN in Section 4.2, each model is developed by performing a parameter sweep and retaining the best architecture or combination of parameters. For MARS, a maximum of 200 piecewise cubic functions are adopted as basis functions. For the RBFN, a Gaussian kernel is employed as the radial function, and a network with three hidden layers and 30 neurons per layer is adopted. Lastly, for Kriging, quadratic basis functions and an anisotropic Gaussian correlation function are adopted. Both the ANN and RBFN were trained using the MATLAB Neural Network Toolbox, while the MARS model was trained using ARESLab (Jekabsons 2016) and the Kriging model using UQLab (Lataniotis et al. 2018)

The comparison between the ANN and the three other surrogate modeling techniques is detailed in Table 3. This table presents the R^2 values between the predicted outputs and the *LS-Dyna* results for the test dataset, the mean error for nonzero pressure points in the test dataset, and the computational time to estimate the hydrodynamic pressure distribution around an AST. The comparison indicates that the ANN has the best performance in terms of both accuracy and computational time. While the Kriging model has a similar accuracy, its computational time is two orders of magnitude greater than that of the ANN. The RBFN model also has a reasonable accuracy, but the mean error is slightly larger than the ANN and Kriging models. Finally, MARS has a large mean error and does not seem to be a suitable model. These results highlight the adequacy of using an ANN to efficiently estimate pressure distributions around ASTs in place of complex and expensive FE analyses.

Table 3: Comparison between the surrogate models

Model	R^2	*Mean error*	*Comp. time*
ANN	*0.999*	*5.4 %*	*0.3 s*
MARS	*0.828*	*25.5 %*	*1.2 s*
RBFN	*0.998*	*9.2 %*	*0.3 s*
Kriging	*0.978*	*6.3 %*	*489 s*

5. ERROR MODELS FOR RELIABILITY ANALYSIS

Even though the ANN model provides an efficient way to estimate hydrodynamic pressures, it is still an approximation of the pressures from the FE model, and a rigorous reliability or fragility analysis should propagate the modeling error associated with this surrogate model. While it may be possible to derive an error model for P_d around ASTs, this study instead derives error models for quantities in the limit state functions that depend on the ANN. This simpler approach does not require modeling the correlation between the pressure errors at each point (θ, h) on an AST.

As noted earlier, two failure modes are possible for ASTs: dislocation or buckling. The limit state function for dislocation is (Bernier and Padgett 2018b):

$$g_{disl} = \begin{cases} W - F_b \\ (W - F_b)\, D/2 - M_{hd} \\ (W - F_b)\, \varphi - F_{hd} \end{cases} \tag{3}$$

where, W is the AST and internal liquid self-weight; F_b is the buoyant force from the surge; F_{hd} and M_{hd} are the horizontal force and overturning moment from the hydrodynamic pressures; and φ is the friction coefficient at the tank foundation. This equation indicates that dislocation can occur due to uplift, overturning, or sliding.

In the case of buckling, the limit state is:

$$g_{buck} = \lambda_{cr} - 1 \tag{4}$$

where λ_{cr} is the critical load factor obtained from a FE buckling analysis. As detailed in Bernier and

Padgett (2018a), buckling is assessed by scaling the loads acting on the AST by a factor λ, and then increasing this factor until the tank shell buckles; a λ_{cr} value less than one indicates buckling.

In Eqs. (3) and (4), only three terms depend on the ANN: F_{hd}, M_{hd}, and λ_{cr}. The error models are derived by computing these three terms by directly using the outputs of the FE analyses for the 240 samples generated in Section 2, and then evaluating these terms using the ANN surrogate model for the same samples. For F_{hd} and M_{hd}, the errors are also normalized by the FE output given the wide scatter of forces and moments. A normal distribution is then assumed to model the errors. The three error models are presented in Table 4, and the error distribution for λ_{cr} is shown in Figure 6. The validity of the normal distributions is confirmed using Kolmogorov-Smirnov tests with a 5% significance level for ε_{Fhd} and ε_{Mhd}, and a 1% level for $\varepsilon_{\lambda cr}$. Moreover, the relatively small standard deviations in Table 3 further highlight the adequate predictive capability of the ANN. Errors associated with the ANN can now be propagated in a reliability analysis by multiplying F_{hd} and M_{hd} in Eq. (3) by $1+\varepsilon_{Fhd}$ and $1+\varepsilon_{Mhd}$ respectively and by adding $\varepsilon_{\lambda cr}$ to λ_{cr} in Eq. (4).

Table 4: Error models for reliability analysis

Model	*Unit*	*Distribution*
ε_{Fhd}	%	*Normal(0.00, 4.24)*
ε_{Mhd}	%	*Normal(0.00, 6.30)*
$\varepsilon_{\lambda cr}$	-	*Normal(-0.01, 0.03)*

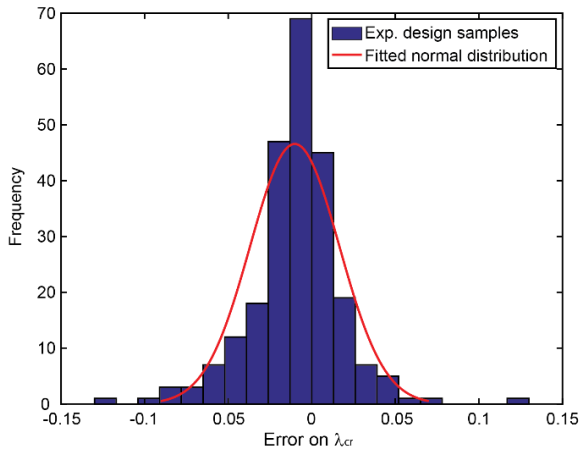

Figure 6: Histogram of errors on λ_{cr} and normal fit.

6. CONCLUSIONS

This study aimed to develop a computationally efficient and accurate surrogate model to estimate hydrodynamic pressures on ASTs subjected to storm surge and wave loads. Using a space-filling sampling method, a series of computational fluid dynamics FE analyses were performed to compute hydrodynamic pressure distributions on ASTs. With the results of the FE analyses, an ANN was trained to predict the hydrodynamic pressure around ASTs as a function of the AST geometry and surge and wave conditions. Against test data, the derived ANN was shown to have an adequate accuracy and predictive capability with a mean error of approximately 5% and a coefficient of determination of almost 1.0. Compared with other surrogate modeling techniques commonly used in civil engineering and structural response prediction applications, the ANN had the best performance in terms of both accuracy and computational time. With the ANN, less than 0.5 seconds are required to estimate the hydrodynamic pressure distribution around an AST, compared to at least 30 CPU hours using an FE analysis. This study also presented simple models to propagate the error associated with the ANN in a fragility or reliability analysis. The small standard deviation of the derived error models further highlighted the adequate predictive capability of the ANN to estimate hydrodynamic loads on ASTs.

Overall, this study demonstrated that the derived ANN is an efficient surrogate to estimate pressure distributions around ASTs in place of complex and expensive FE analyses. The ANN surrogate model coupled with the error models proposed in this paper will now enable and facilitate future sensitivity, fragility, and reliability studies across a broad range of AST geometry and storm surge conditions. Future work will also focus on improving the accuracy of the ANN in regions of high pressures, which are more critical to assess adequately buckling and dislocation than regions of low pressures.

7. ACKNOWLEDGEMENT

The authors acknowledge the financial support of the National Science Foundation under award #1635784. The first author was also supported in part by the Natural Sciences and Engineering Research Council of Canada. The authors thank Prof. Clint Dawson for providing the ADCIRC+SWAN results. The computational resources were provided by the Big-Data Private-Cloud Research Cyberinfrastructure MRI-award funded by NSF under grant CNS-1338099 and by Rice University. Any opinions, findings, and conclusions or recommendations expressed in this paper are those of the authors and do not necessarily reflect the views of the sponsors.

8. REFERENCES

Bernier, C., Elliott, J. R., Padgett, J. E., Kellerman, F., and Bedient, P. B. (2017). "Evolution of Social Vulnerability and Risks of Chemical Spills during Storm Surge along the Houston Ship Channel." *Natural Hazards Review*, 18(4), 1–14.

Bernier, C., and Padgett, J. (2018a). "Buckling of aboveground storage tanks subjected to storm surge and wave loads." *Engineering Structures*.

Bernier, C., and Padgett, J. E. (2018b). "Forensic investigation of aboveground storage tank failures during Hurricane Harvey using fragility models." *Forensic Engineering 8th Congress*.

Chen, Y., Kopp, G. A., and Surry, D. (2002). "Interpolation of wind-induced pressure time series with an artificial neural network." *Journal of Wind Engineering and Industrial Aerodynamics*, 90(6), 589–615.

Chojaczyk, A. A., Teixeira, A. P., Neves, L. C., Cardoso, J. B., and Guedes Soares, C. (2015). "Review and application of Artificial Neural Networks models in reliability analysis of steel structures." *Structural Safety*, Elsevier Ltd, 52(PA), 78–89.

Dawson, C. (2017). "The Computational Hydraulics Group." <http://chg.ices.utexas.edu>.

Fenton, J. D. (1988). "The numerical solution of steady water wave problems." *Computers and Geosciences*, 14(3), 357–368.

Godoy, L. (2007). "Performance of storage tanks in oil facilities damaged by Hurricanes Katrina and Rita." *Journal of Performance of Constructed Facilities*, 21(6), 441–449.

Godoy, L. A. (2016). "Buckling of vertical oil storage steel tanks: Review of static buckling studies." *Thin-Walled Structures*, Elsevier, 103, 1–21.

Hurtado, J. E., and Alvarez, D. A. (2001). "Neural-network-based reliability analysis: A comparative study." *Computer Methods in Applied Mechanics and Engineering*, 191(1–2), 113–132.

Jekabsons, G. (2016). *ARESLab: Adaptive Regression Splines toolbox for Matlab/Octave*.

Jin, R., Chen, W., and Simpson, T. W. (2001). "Comparative studies of metamodelling techniques under multiple modelling criteria." *Structural and Multidisciplinary Optimization*, 23(1), 1–13.

Lataniotis, C., Marelli, S., and Sudret, B. (2018). *UQLab User Manual - Kriging*.

Lee, T. L. (2006). "Neural network prediction of a storm surge." *Ocean Engineering*, 33(3–4), 483–494.

Livermore Software Technology Corporation. (2016). "LS-Dyna R8.0.0."

Luettich, R. A., and Westerink, J. J. (2004). "Advanced Circulation Model for Oceanic, Coastal and Estuarine Waters."

Mase, H., and Kitano, T. (1999). "Prediction model for occurrence of impact wave force." *Ocean Engineering*, 26(10), 949–961.

MathWorks. (2016). "MATLAB R2016b." Natick, MA.

Mckay, M. D., Beckman, R. J., and Conover, W. J. (1979). "A Comparison of Three Methods for Selecting Values of Input Variables in the Analysis of Output from a Computer Code." *Technometrics*, 21(2), 239–245.

Morison, J. R., Johnson, J. W., and Schaaf, S. A. (1950). "The Force Exerted by Surface Waves on Piles." *Journal of Petroleum Technology*, 2(05), 149–154.

Sengul, H., Santella, N., Steinberg, L. J., and Cruz, A. M. (2012). "Analysis of hazardous material releases due to natural hazards in the United States." *Disasters*, 36(4), 723–743.

Tsai, J. C., and Tsai, C. H. (2009). "Wave measurements by pressure transducers using artificial neural networks." *Ocean Engineering*, Elsevier, 36(15–16), 1149–1157.

Wang, C. Z., and Wu, G. X. (2010). "Interactions between fully nonlinear water waves and cylinder arrays in a wave tank." *Ocean Engineering*, Elsevier, 37(4), 400–417.